

Under the Dome: A 3D Urban Texture Model and Its Relationship with Urban Land Surface Temperature

Qingfeng Guan, Yao Yao, Teng Ma, Ye Hong, Yongpan Bie & Jianjun Lyu

To cite this article: Qingfeng Guan, Yao Yao, Teng Ma, Ye Hong, Yongpan Bie & Jianjun Lyu (2021): Under the Dome: A 3D Urban Texture Model and Its Relationship with Urban Land Surface Temperature, *Annals of the American Association of Geographers*, DOI: [10.1080/24694452.2021.1972790](https://doi.org/10.1080/24694452.2021.1972790)

To link to this article: <https://doi.org/10.1080/24694452.2021.1972790>



Published online: 03 Nov 2021.



Submit your article to this journal [↗](#)



View related articles [↗](#)



View Crossmark data [↗](#)

Under the Dome: A 3D Urban Texture Model and Its Relationship with Urban Land Surface Temperature

Qingfeng Guan,^{*}  Yao Yao,^{*}  Teng Ma,^{*} Ye Hong,[†] Yongpan Bie,^{*} and Jianjun Lyu^{*} 

^{*}*School of Geography and Information Engineering National Engineering Research Center of GIS, China University of Geoscience, Wuhan, China*

[†]*Institute of Cartography and Geoinformation, ETH Zurich, Switzerland*

The spatial distribution of buildings is one of the key factors influencing the local environment within a city. The quantitative measurement of building distribution can provide critical information for exploring local climate patterns in urban areas. Previous studies mainly focused on the two-dimensional spatial distribution of buildings and ignored the differences in height. In this study, a three-dimensional (3D) urban texture model based on an improved radial distribution function is proposed to describe the 3D spatial distribution of urban buildings. Using a set of concentric domes above the ground, a texture curve can be generated at any location in a city, from which a variety of numerical features are extracted to depict the local 3D urban landscape quantitatively. The proposed model was applied to Wuhan, one of the largest cities in central China, and the results demonstrated that the proposed model could identify various building distribution patterns in the city. Additionally, the relationship between urban texture and land surface temperature in Wuhan was analyzed. It was found that the 3D urban texture model effectively improved the accuracy of land surface temperature estimation. This study provides a new tool for urban environmental assessment and urban planning decision making. *Key Words: 3D urban texture model, radial distribution function, urban structure, urban surface temperature.*

Disorganized urban spatial structure can lead to a series of environmental problems such as local climate change and urban heat islands (UHIs; Sossa et al. 2013; Leconte et al. 2015). Hence, in recent years, accurately describing urban spatial structures at fine scales and exploring the relationships between spatial structures and local environments have become the focus of urban research (Brian 2008; Xian 2008; Kumar and Tretkoff 2010), which has far-reaching significance for the sustainable development of cities (Strømman-Andersen and Sattrup 2011; Inostroza, Baur, and Csaplovics 2013).

A city is a complex system, in which buildings play a key role to form the spatial structure of the city (Jian et al. 2012; Quattrochi 2013). The distribution of buildings can reflect the layout characteristics of urban spatial structures, which are defined as urban building textures (Dobinson 1993; Heinzel and Kemper 2015). The term *texture* is often used in remote sensing applications to describe the features of the detailed structure of an object's surface (Gaetano, Scarpa, and Poggi 2009), and the

quantitative extraction of these features can effectively help distinguish different types of ground objects (Li et al. 2017). The concept of urban texture was first proposed by Rykwert (1988) and was defined as the pattern of building distribution in a city. The distribution of various urban textures is then regarded as the texture morphology. Previously, Ai and Zhang (2007) studied urban texture based on the distribution characteristics of buildings by calculating the statistical features of buildings. The spatial variation of urban land was measured using statistical features such as the building footprint and density. Later, other scholars analyzed building texture and landscape morphological characteristics by extracting building objects and quantifying building density (B. Yu et al. 2010; Z. Chen and Soh 2014). These studies focused on urban morphology by calculating the two-dimensional (2D) urban morphological features (Pan et al. 2008) and urban morphological evolution and prediction (Y. He et al. 2015) and often ignored the variations in building height. As the built space gradually extends to the sky, the urban texture has significant three-dimensional (3D) features that

affect the local environment of a city (Ivanova 2015; Zhu and Sun 2017).

The past decade has seen an increased number of studies on the 3D forms of cities (Z. He et al. 2020). Geographical information systems and high-resolution remote sensing images were combined to extract the 3D features of buildings for quantifying 3D urban expansion (X. Yang and Li 2013; Qin et al. 2015). With the recent acceleration of urbanization in China, a large number of buildings and roads have been built in urban areas (Y. Zhang et al. 2018). The modifications of the material properties and geometries of infrastructures have led to significant changes in the physical processes on the Earth's surface, resulting in notable local environmental consequences such as UHIs (Roman et al. 2016; Yin et al. 2018). The vertical growth of the urban space has been found to intensify the thermal environment in a city (Perini and Magliocco 2014). Therefore, scholars have discussed the microclimates and UHIs in cities by quantifying the building density (Guo et al. 2016) and designing 3D urban surface models (Luo and Li 2014).

The primary objective of studying the texture morphology of buildings is to quantify the building form accurately and to reveal its relevance to the local climate, UHIs, and other environmental issues of cities (Strømman-Andersen and Sattrup 2011; Palme, Inostroza, and Salvati 2018). The microclimate variations in a city have a direct relationship with the spatial distribution of local buildings. Previous studies mainly calculated the statistical features of buildings at the urban scale. They expounded the correlation using elements related to the urban environment while ignoring the relationship between the environment and the texture morphology of local building spaces (or building groups). Stewart and Oke's (2012) study on the local climate zone (LCZ) showed that building layout in a 3D space has significant impacts on local urban climate. They suggested that in a built environment zone, according to the spatial distribution characteristics of buildings, the climate zone can be divided according to whether the buildings are high-rise or low-rise and compact or open. The buildings in a city are highly mixed in terms of height and spatial arrangement, however. Simple features (e.g., high- or low-rise and compactness) can hardly reflect the complex patterns of spatial distribution of buildings, providing only limited information for LCZ analysis and other urban environmental investigations.

Therefore, there are two main problems in the study of buildings' spatial form in cities at present: (1) Most of the studies have focused on either the building scale or regional scale, ignoring the local building space. Buildings generally exist in the form of groups (Kharchenko 2016). Different building groups have different morphological characteristics (Sobstyl et al. 2018), which is an essential factor to be considered in urban planning and the main reason for the formation of local climate in a city (Stewart and Oke 2012). (2) Even though a few studies have paid attention to the distribution characteristics of building groups, the quantitative features used in these studies, such as the local building density (X. Yang and Li 2015) and sky view factor (L. Chen et al. 2012), focused on limited aspects of spatial distribution of buildings and can hardly reflect the complex 3D texture morphology of a building group. An effective quantitative method for describing the 3D texture morphologies of building groups is therefore needed.

Analogous to the complex structure in a microscopic system, in which the ordered and disordered arrangements of particles constitute substances with different states of existence (Bragg and Lipson 1938), the ordered and disordered distributions of buildings constitute the varying local urban landscapes (Manesh and Tadi 2011). By adopting the radial distribution function (RDF) to quantitatively describe the distribution patterns of building groups in a 2D space, Sobstyl et al. (2018) examined the 2D building textures at various locations in a city and found that the regularity degree of spatial arrangement of a building group had a significant impact on the local temperature. The RDF had been initially used in physics to describe the spatial structures of particle arrangements of substances (Burgot 2017), such as crystals with regular structures and liquids or amorphous substances with irregular structures (Sukhomlinov and Müser 2017). Sobstyl et al.'s (2018) study showed that the texture characteristics (or texture morphologies) of buildings arranged with high regularity are similar to the those of crystals, whereas the texture characteristics of buildings arranged with low regularity are similar to the those of fluids. Here, high regularity means that buildings are arranged in a 2D space in an orderly pattern with a clean layout plan, and low regularity means the buildings are more randomly distributed without an obvious pattern. They also found that

these texture morphologies are related to the formation of UHIs.

Even though Sobstyl et al. (2018) demonstrated the applicability of RDF in describing the texture morphologies of building groups in cities and analyzed the relationship between urban texture and urban environment, their study was conducted in a 2D space and the variation of building height was ignored. Three-dimensional texture features are essential to comprehensively and accurately characterize the complex patterns of spatial distributions (including 2D arrangements and height variations) of building groups (Jian et al. 2012; X. Yang and Li 2015; Wentz et al. 2018). Therefore, the effective extraction and quantitative representation of 3D texture features of buildings are the key foundation to unearth the relationship between the urban spatial structure and urban environment (Ellefsen 1991; S. Yu et al. 2016; Palme, Inostroza, and Salvati 2018).

This study proposes a 3D urban texture model based on an improved RDF to quantitatively characterize the 3D texture morphologies of built-up environments in cities. For a specific location in an urban area, the RDF treats buildings as particles, and generates a texture curve that abstracts the 3D spatial distribution of buildings. A collection of quantitative features can then be extracted from the texture curve to represent the morphological characteristics of the 3D landscape. By applying the proposed RDF-based model to Wuhan, a megacity in China, we analyzed the distributions of building groups with different texture morphologies. Moreover, the correlation between 3D texture morphology and land surface temperature (LST) in Wuhan was analyzed. The proposed model is a new approach for quantitatively extracting the 3D characteristics of spatial distribution of buildings and can provide key information for analyzing the relationship between built landscape and local environment in urban areas.

Method

The overall flowchart of this study is shown in Figure 1. Using the data set of 3D building models, the proposed RDF-based model generates the urban texture curves at various locations in the city to represent the 3D distribution patterns of local buildings. A set of quantitative features is extracted from each texture curve to characterize the built landscape at

the corresponding location, such that the texture morphology of a local building group can be distinguished. These 3D texture features are then used to estimate the LSTs at the corresponding locations through the random forest regression (RFR) method to illustrate the correlation between 3D urban texture and local environment in urban areas.

RDF-Based 3D Urban Texture Model

The 3D urban texture model based on RDF is proposed in this study to generate the urban texture curve at any location in the city to reflect the 3D spatial distribution pattern of local buildings. As mentioned before, the RDF was initially used in physics to describe the spatial structures of particle arrangements of substances. As shown in Figure 2A, in a microscopic 3D space, the RDF calculates the probability $g(r)$ of other particles appearing around an arbitrarily designated “central” particle within a radius r (Bragg and Lipson 1938; Burgot 2017); that is, the ratio of the regional density of particles in the boundary range (i.e., the density of particles in a spherical shell with a thickness of δr) to the global density (i.e., the density of particles within a sphere with a radius of r). Using multiple concentric spheres with a radius interval of δr , a curve of $g(r)$ can be generated to reflect the spatial structure of particles; that is, the spatial variation of probabilities of other particles appearing around the “central” particle at different distances.

In the proposed 3D urban texture model, the particles are replaced by buildings. Also, given that the purpose of this model is to describe the spatial distribution patterns of aboveground buildings in urban areas, the center of concentric spheres is located on and above the ground and only the buildings above the ground are considered. As shown in Figure 2B, using a specific location “C” as the center, a set of concentric spheres are constructed, and the building density in each spherical shell formed by two adjacent spheres is calculated to generate the urban texture curve of local urban landscape. The radius r of the local building group (i.e., the radius of the largest sphere) can be determined according to different research purposes. After r is determined, the best δr value can be obtained through experiments. The value of $g(r)$ of each spherical shell is calculated as follows:

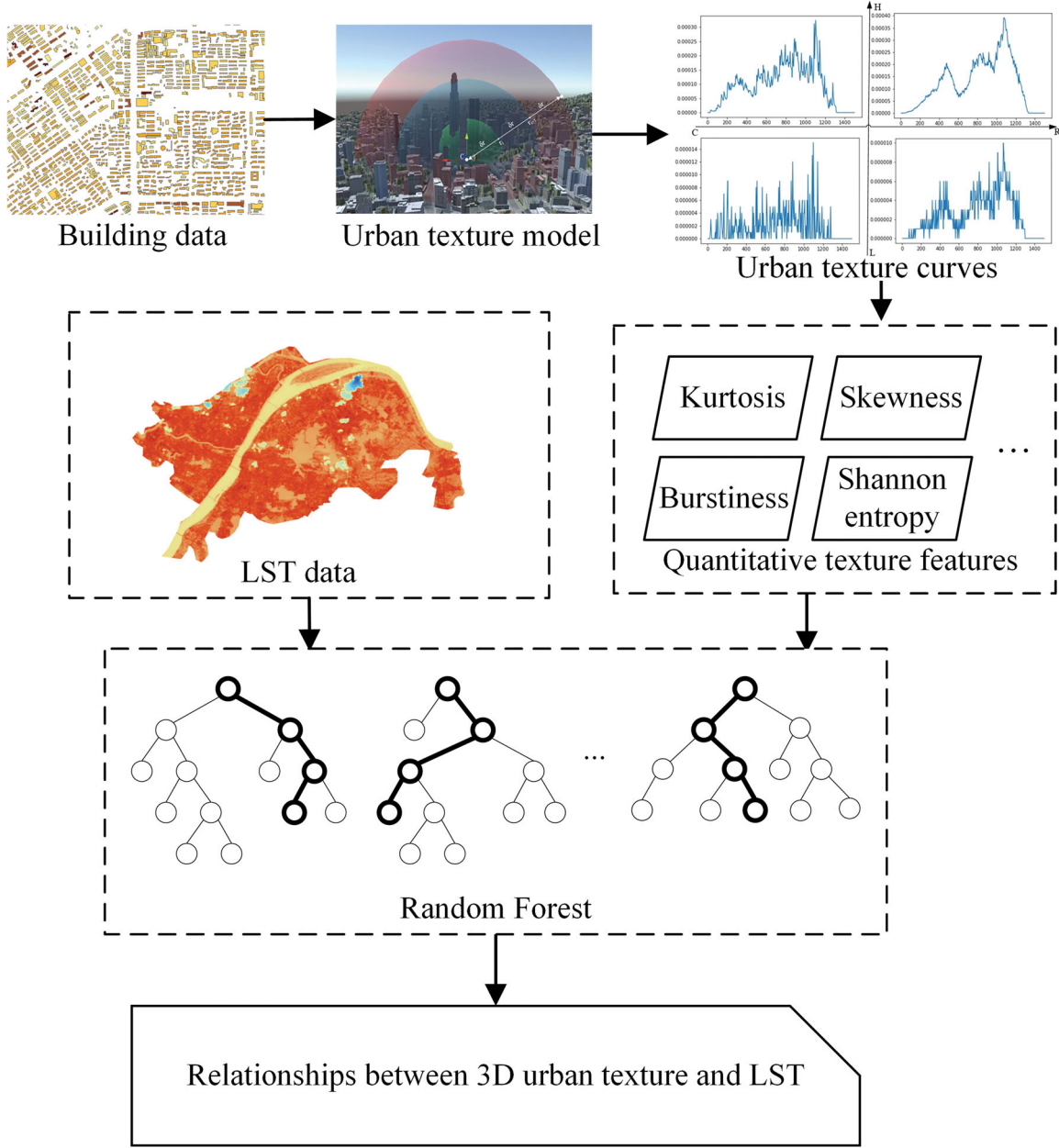


Figure 1. The methodological flowchart. Note: LST = land surface temperature.

$$g(r_i) = \frac{\rho_{\delta r(i,i+1)}}{\rho_{r_i}} = \frac{1}{\rho_{r_i}} \frac{v_{\delta r(i,i+1)}}{V_{\delta r(i,i+1)}}, \quad (1)$$

where ρ_{r_i} represents the global density of the buildings within the sphere with a radius of r_i and $\rho_{\delta r(i,i+1)}$ represents the regional density of the buildings within the i th spherical shell with a thickness of δr . $v_{\delta r(i,i+1)}$ represents the volume of the buildings within the i th spherical shell, and $V_{\delta r(i,i+1)}$ represents the total volume of the i th spherical shell. When a building intersects with one or more spheres, only the proportion of the building's volume

within the intersecting sphere or spherical shell is considered for the density calculation. Thus, both the spatial arrangement and heights of buildings (i.e., the key fundamental components of local urban morphology) are taken into account in the proposed 3D urban texture model.

For the convenience of calculation, this study regards a building as a regular 3D structure when estimating its volume and does not consider complex forms such as building roofs and irregular facades. The intersection points between the central axis of the building and the spheres are first determined and

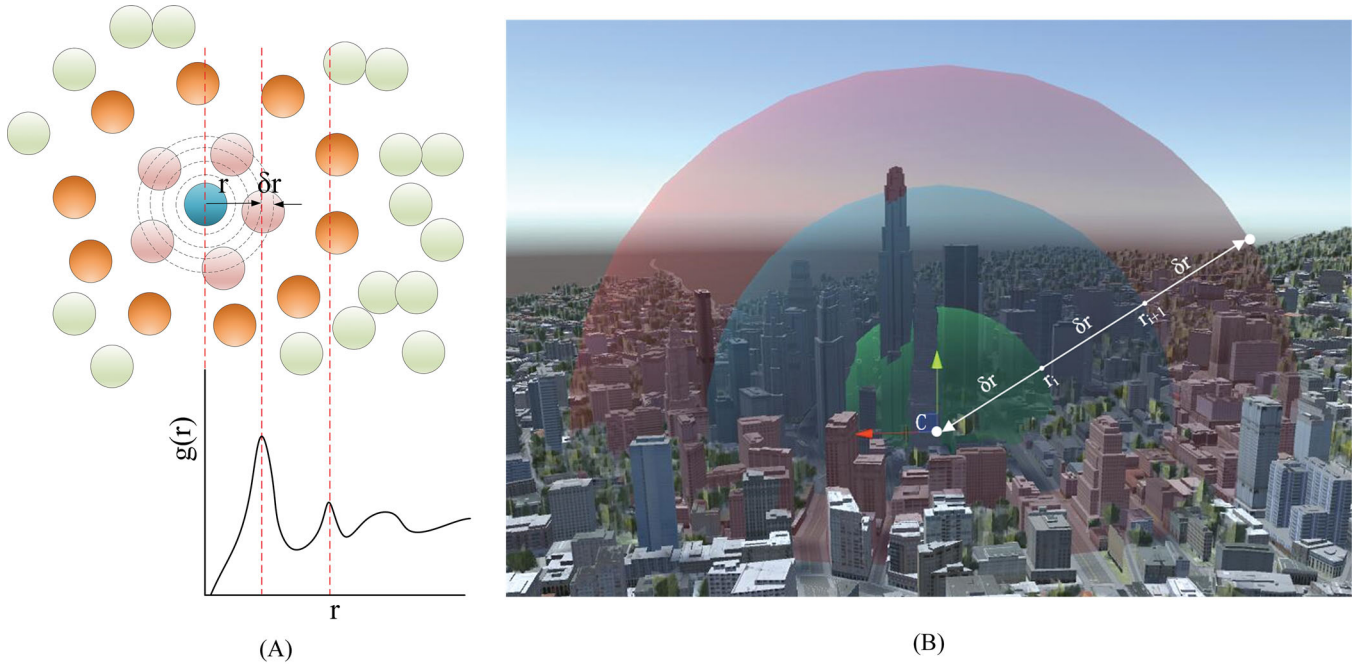


Figure 2. (A) Schematic diagram of the relationship between radial distribution function and particle structure; (B) the radial distribution function–based 3D urban texture model proposed in the study.

the volumes of the building intercepted by the spheres are then calculated based on the heights of the intersections and the building footprint area.

As mentioned earlier, in the proposed model, the center of the concentric spheres is located on or above the ground, because only the aboveground buildings are considered in the generation of the texture curve. To explore whether the height of the spherical center influences the resultant curve, a series of experiments was conducted with various center heights ranging from 0 to 100 m in a typical urban area. As shown in [Figure 3](#), as the height of the center increases, the shape of the curve hardly changes. That is, the height of the spherical center does not affect the texture curve significantly. Therefore, this study places the spherical center on the ground; that is, the height is set to 0 m. In other words, the proposed model uses a set of concentric domes on the ground to generate the urban texture curve of the aboveground buildings at a specific location in a city.

Therefore, the proposed model can derive a simple and abstract representation (i.e., urban texture curve) of the complex 3D spatial distribution of a group of buildings from the original 3D models of buildings. Quantitative features can then be extracted from such a curve to characterize the 3D texture morphology of the local urban landscape.

Feature Extraction from the Urban Texture Curve

In physics, to help understand and analyze the particle arrangement in microscopic systems and differentiate various types of substances, quantitative features can be extracted from the RDF curve to represent the characteristics of the spatial arrangement of particles for physical interpretation. For example, the first peak of the RDF curve represents the bonding strength among the particles, and a sharper shape of this peak indicates that the center particle and the nearest neighboring particle have a stronger bonding strength (Cherkas and Cherkas 2016). The integral from the origin to the first peak position represents the nearest coordination number of the central particle. In a microscopic system, the coordination number describes the tightness of the arrangement of the particles in the system. The larger the coordination number is, the closer the particles are arranged (Bragg and Lipson 1938).

Similarly, quantitative features can be extracted from an urban texture curve to describe various characteristics of the 3D spatial distribution pattern of a group of buildings. In this study, ten features are extracted, including three data features and seven curve features ([Table 1](#)). Hence, quantitative analysis and comparisons can be carried out using these features to explore the urban texture morphologies

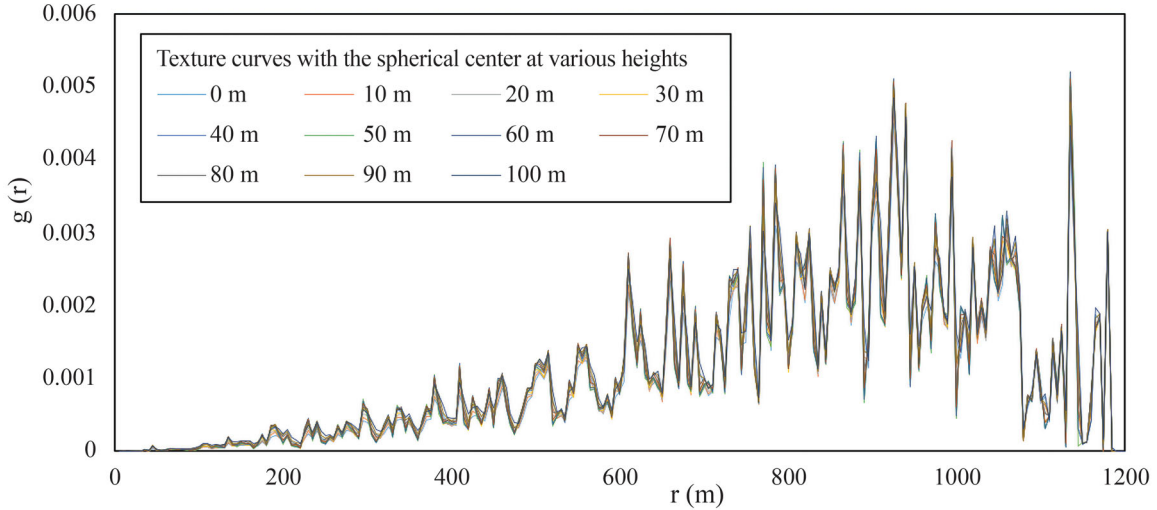


Figure 3. Urban texture curves with spherical center at various heights.

Table 1. Features extracted from an urban texture curve

	Features	Description
Data features	Coefficient of variation (CV)	$CV = \frac{\alpha}{\mu}$, which reflects the absolute value of the degree of data dispersion. α and μ are the standard deviation and average value of data, respectively. A distribution with a CV greater than 1 is a distribution with high differences (Brown 2011).
	Burst statistics (B)	$B = \frac{\alpha - \mu}{\alpha + \mu}$, which can be used to measure the burstiness of the spatial distribution. α and μ are the standard deviation and average value of data, respectively. A B close to -1 indicates that the data has strong burstiness, and close to 1 indicates that the data are regular and predictable (Goh and Barabási 2012).
	Shannon entropy (Sh)	$Sh = -\sum_{i=1}^n p_i \log p_i$, which can be used to measure the uncertainty or disorder of the system. p_i is the probability of event i . A large Sh value indicates that the uncertainty of the information source is large (Shannon, Weaver, and Wiener 1949).
Curve features	Skewness (Sk)	$Sk = \frac{1}{n\alpha^3} \sum_{i=1}^n (x_i - \mu)^3$, which can describe the degree of symmetry of the distribution's deviation. α and μ are the standard deviation and average value of data, respectively. $Sk > 0$ represents a right-skewed distribution, and $Sk < 0$ represents a left-skewed distribution (Mardia 1970).
	Kurtosis (K)	$K = \frac{1}{n\alpha^4} \sum_{i=1}^n (x_i - \mu)^4$, which describes the degree of abruptness. α and μ are the standard deviation and average value of data, respectively. Under the same standard deviation, the larger the kurtosis is, the more extreme and the steeper the distribution (Mardia 1970).
	The first peak (FP)	Radius r at the first peak.
	The maximum peak (MP)	Radius r at the maximum peak.
	The first peak area (FPA)	The integral from the origin to the first peak position, which is used to describe the extent to which other particles are bound around the center particle (Burgot 2017). In this study, buildings are considered as particles in a system.
	The maximum peak area (MPA)	The integral from the origin to the maximum peak position, indicating the degree of binding of all particles to the central particle (Burgot 2017). In this study, particles are replaced by buildings.
	Transition point (Tg)	$Tg = \frac{g_{\max}}{g_{\min}}$, which is the ratio of the first peak (g_{\max}) to the first valley (g_{\min}). The larger Tg is, the stronger the dependence between particles (Burgot 2017). In this study, particles are replaced by buildings.

in a complex urban landscape, which can hardly be done using the original 3D models of buildings. Various spatial distribution patterns of buildings can be identified because they exhibit distinguishing texture morphologies, and their relationships with the local environment (such as land surface temperature) can be evaluated.

Correlation Analysis with LST

The difference in the shape of built space greatly affects the temperature variation in an urban area (Sobstyl et al. 2018). In this study, the correlation between urban texture morphology and LST is explored through an RFR model. It is worth noting that the correlations between urban texture morphology and other environmental variables (e.g., air quality and noise) can also be analyzed through such an approach.

Because previous studies suggested that the best range for an LCZ is between 200m and 500m (Stewart and Oke 2012), we take 500m as the maximum range r to ensure that the LSTs in the area have the same characteristics and that the area under the dome can form a suitable LCZ (Luo and Li 2014). We regard each sampling point and its surrounding 500-m radius as an LCZ and generate a texture curve based on the proposed model. We use the texture features in each LCZ to fit the LST of the center sampling point, creating 10,000 training sets. Moreover, we set up different radius gaps to explore the best configuration (from 5m–100m with an interval of 5m). The scikit-learn package based on the Python language (Kramer 2016) is used to implement the RFR fitting.

The RFR is an integrated decision tree consisting of a set of unrelated regression decision trees $\{h(x, \theta_t), t = 1, 2, 3, \dots, T\}$ (Cutler, Cutler, and Stevens 2011), and the formula is as follows:

$$h(x) = \frac{1}{N} \sum_{n=1}^T \{h(x, \theta_t)\}, \quad (2)$$

where θ_t is an independent and identically distributed random vector, x is the input vector, and T is the number of decision trees. In this study, T is set as 50.

The goodness of fit (R^2) is used to describe the fitting accuracy between LST and 3D texture features. R^2 can test the fitting effect of the regression model to sample data, and an R^2 close to one

indicates that the regression model has a good fit. The formula for calculating R^2 is as follows (Grömping 2009):

$$R^2 = \frac{\sum_{i=1}^n (\hat{y}_i - \bar{y})^2}{\sum_{i=1}^n (y_i - \bar{y})^2}, \quad (3)$$

where y_i is the obtained actual temperature, \hat{y}_i is the predicted surface temperature using the model, \bar{y} is the average value of the obtained actual temperature, and n represents the sample size.

The influence of each feature on the LST is further investigated by calculating the average contribution of each feature using the Gini index or the out-of-bag error rate (Cutler, Cutler, and Stevens 2011).

Data Sets for Experiments

To demonstrate the proposed 3D urban texture model's capabilities for extracting urban texture features and distinguishing various texture morphologies, a series of experiments was conducted using two data sets: a simulated data set that includes building groups with highly distinguishable texture morphologies and a real-world data set that represents complex urban landscapes. The real-world data set was also used in experiments to explore the relationship between 3D urban texture and LST.

Simulated Building Data Set

To verify whether the texture curve derived by the proposed RDF-based model has significantly distinguishable characteristics for various spatial patterns of local urban landscapes, we simulated two types of building groups: buildings with high regularities (R-type) and buildings with low regularities (C-type). Each category includes three sets of data. As mentioned before, an R-type building group is composed of buildings that are orderly arranged in the 2D space with a clean layout pattern (Figure 4; R1/R2/R3), whereas a C-type group is composed of buildings that are randomly scattered in space without a clean pattern (Figure 4; C1/C2/C3). The number of buildings in each group ranges from 100 to 200. The heights of buildings can be set according to the purposes of experiments (see the "Results" section for details). The maximum spatial range of these simulation data is 3,000m, meaning that all

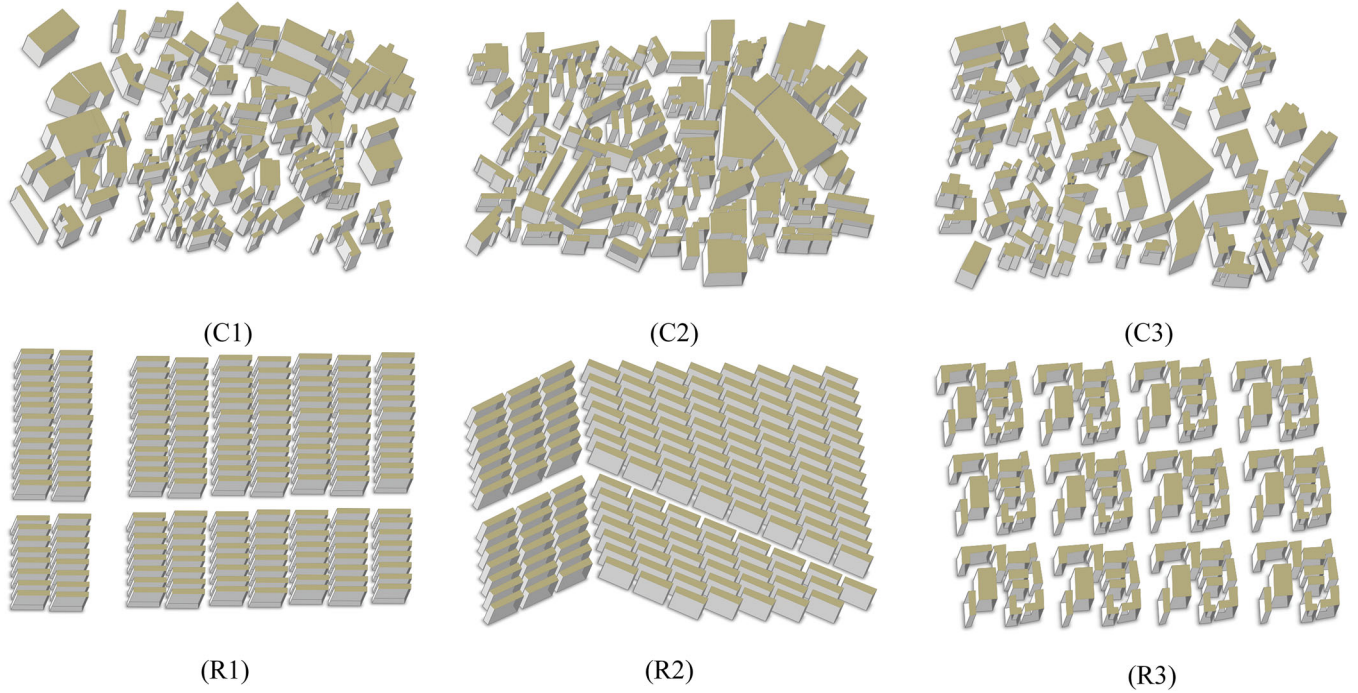


Figure 4. Simulated building data with various texture morphologies.

buildings are included in the dome with a radius of 1,500 m.

It is worth noting that in the real world, a local urban landscape might include one or more clusters of buildings. The simulated data set only includes single-cluster building groups, but the real-world data set (see the next section) includes both single-cluster and multicenter building groups. In a single-cluster building group, all buildings are distributed relatively close to each other, forming one cluster of buildings. In a multicenter group, multiple clusters of buildings exist and each cluster consists of a set of closely distributed buildings that are relatively distant from other clusters of buildings.

Real-World Data Set

To illustrate the performance of the proposed 3D urban texture model and explore its relationship with the local environment (LST in this study), we also applied the model to the central area of Wuhan, Hubei Province, China, a national-level central city that has gone through rapid development in recent years. As shown in Figure 5, the study area is the downtown area of Wuhan ($29^{\circ}58'-31^{\circ}22'N$ and $113^{\circ}41'-115^{\circ}05'E$), which includes seven districts (Hongshan, Jiang'an,

Jiangnan, Wuchang, Qingshan, Hanyang, and Qiaokou).

The rapid economic development of Wuhan in recent years has caused drastic changes in the spatial structure of the urban area, leading to highly complex urban landscapes (e.g., new districts, old towns, and urban villages) with varying spatial patterns of buildings. The original building data set of the study area contains not only the footprints but also the heights of buildings, providing 3D information on the urban landscapes. Some typical urban texture morphologies are shown in Figure 6, including a group of low-rise buildings that are arranged with high regularity (RL), a group of low-rise buildings that are arranged with low regularity (CL), a group of high-rise buildings that are arranged with low regularity (CH), and a group of high-rise buildings that are arranged with high regularity (RH).

To prove that a texture curve carries adequate information to represent the complex texture morphology of the local urban landscape and to explore the relationship between urban texture morphology and local environment, we randomly selected 10,000 locations in the study area and used the texture features of each local building group to estimate the LST at its location.

The LST data for the study area during the daytime on a sunny day (26 July 2017) with a spatial

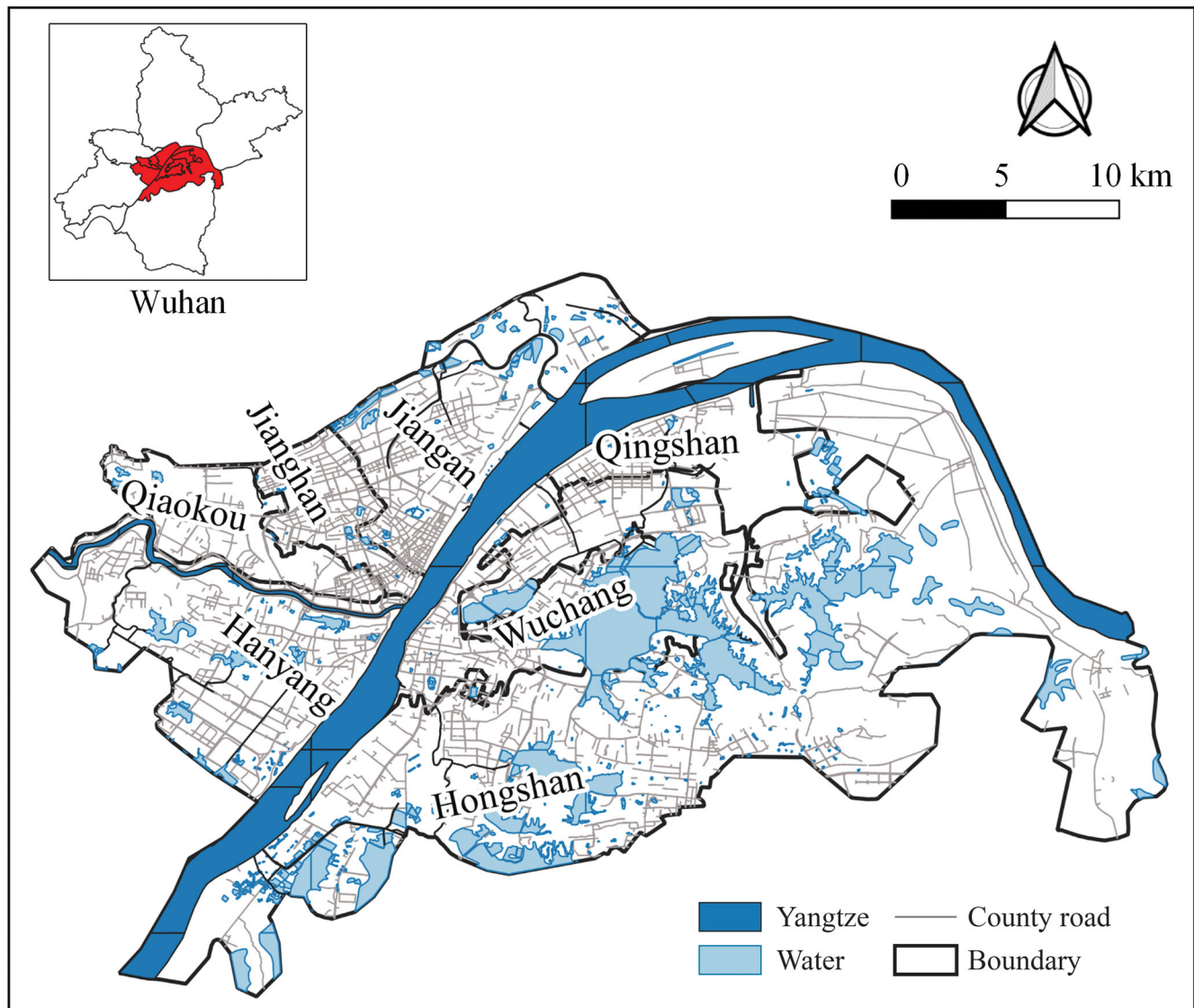


Figure 5. Case study area: Downtown area of Wuhan, Hubei Province.

resolution of 30 m were generated using satellite imagery through a practical single-channel algorithm proposed by Wang et al. (2019). Landsat images (including Landsat 4, Landsat 5, Landsat 7 data, and the first band of Landsat 8 TIRS), the Thermodynamic Initial Guess Retrieval database, and the MODIS/UCSB Emissivity Library were used to derive the LST.

Results

Texture Curves of Simulated Building Data Set

Texture Curves of Single-Cluster Building Groups with Varying Regularities. The proposed

RDF-based model was applied to the simulated building data set to examine the model's capability of distinguishing various regularities of spatial arrangement of building groups. In such an experiment, the height of the simulated buildings was set as 100 m and the radius interval δr for the concentric domes was 5 m.

In microscopic physics, an RDF-derived curve with a smoother shape and exhibiting obvious peaks within a longer range indicates that the particles are arranged with high regularity and the structure is stable, which can often be found in crystals. On the contrary, the RDF curves of fluids are highly fluctuating, indicating chaotic arrangements and unstable structure of particles. Our experiment demonstrated

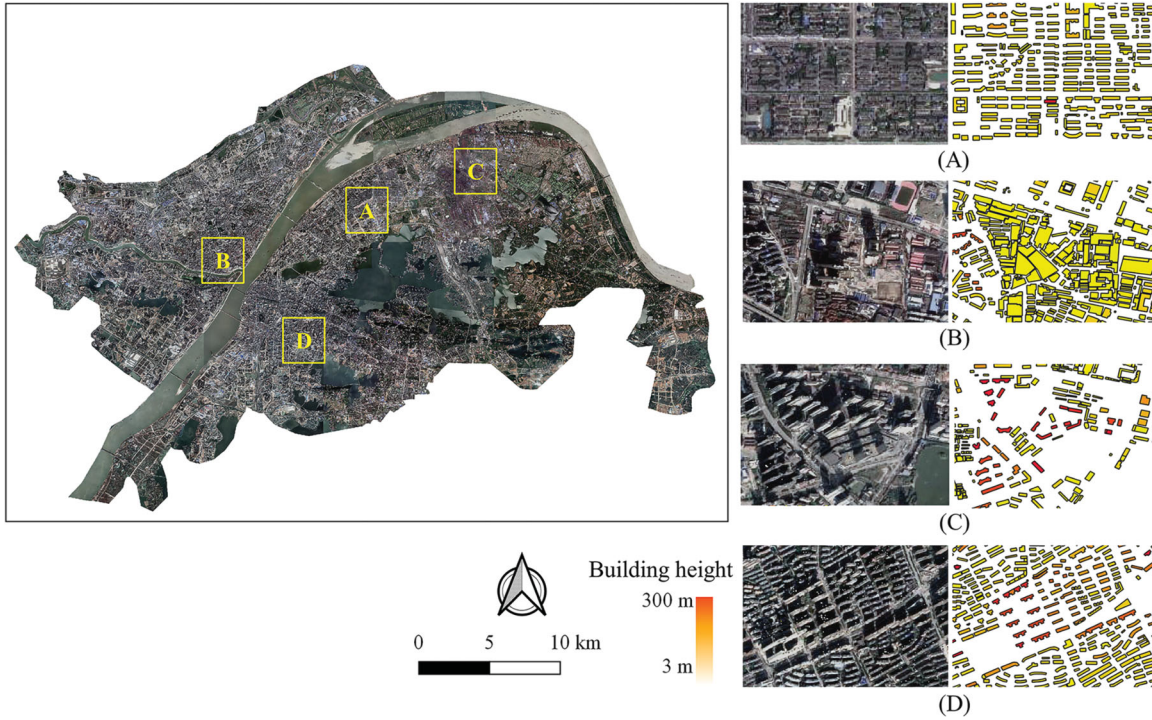


Figure 6. The building footprints in the study area and four typical building groups with various spatial patterns. (A) an area containing a group of low-rise buildings that are arranged with high regularity, (B) an area containing a group of low-rise buildings that are arranged with low regularity, (C) an area containing a group of high-rise buildings that are arranged with low regularity, and (D) an area containing a group of high-rise buildings that are arranged with high regularity.

the same phenomenon in urban landscapes. As shown in Figure 7, the curves of R-type building groups are significantly smoother (i.e., less fluctuating) than those curves of C-type groups, and a distinct peak can be found for the general trend of each R-type curve. Therefore, the shape of urban texture curve derived by the RDF-based model can clearly distinguish the arrangement regularity of building groups.

Texture Curves of Single-Cluster Building Groups with Varying Heights. The heights of buildings can affect the local environment (e.g., temperature) in an urban area (Palme, Inostroza, and Salvati 2018). To explore the change of the curve with various building heights, we set the height of simulated buildings as 6 m, 100 m, 200 m, and 300 m. As shown in Figure 8, the texture curve becomes smoother when the building height increases but the peak position remains unchanged. Therefore, the heights of buildings also affect the shape of a texture curve, indicating the proposed RDF-based texture model can represent the 3D spatial patterns (including 2D arrangements and height variations) of building groups.

The quantitative features extracted from such RDF-derived curves can describe the texture morphologies of local urban landscape.

Real-World Case Study Results

The urban landscape in the real world is much more complex than the simulated data set, but similar patterns can also be found. Various degrees of regularity in the spatial arrangement of buildings were found in Wuhan. Figure 9A shows a building group that is arranged with low regularity, less unified planning, and messy roads (C-type). Figure 9B shows a building group that is arranged with high regularity, the layout plan is unified, and the roads are neat (R-type).

The heights of buildings in Wuhan also vary significantly. High-rise buildings (more than ten floors, >30 m) and low-rise buildings (one to six floors, 3–18 m) are widely scattered in the urban area. We found a large number of building groups that include mostly high-rise buildings (H-type), such as central business districts, or mostly low-rise buildings (L-type), such as urban villages.

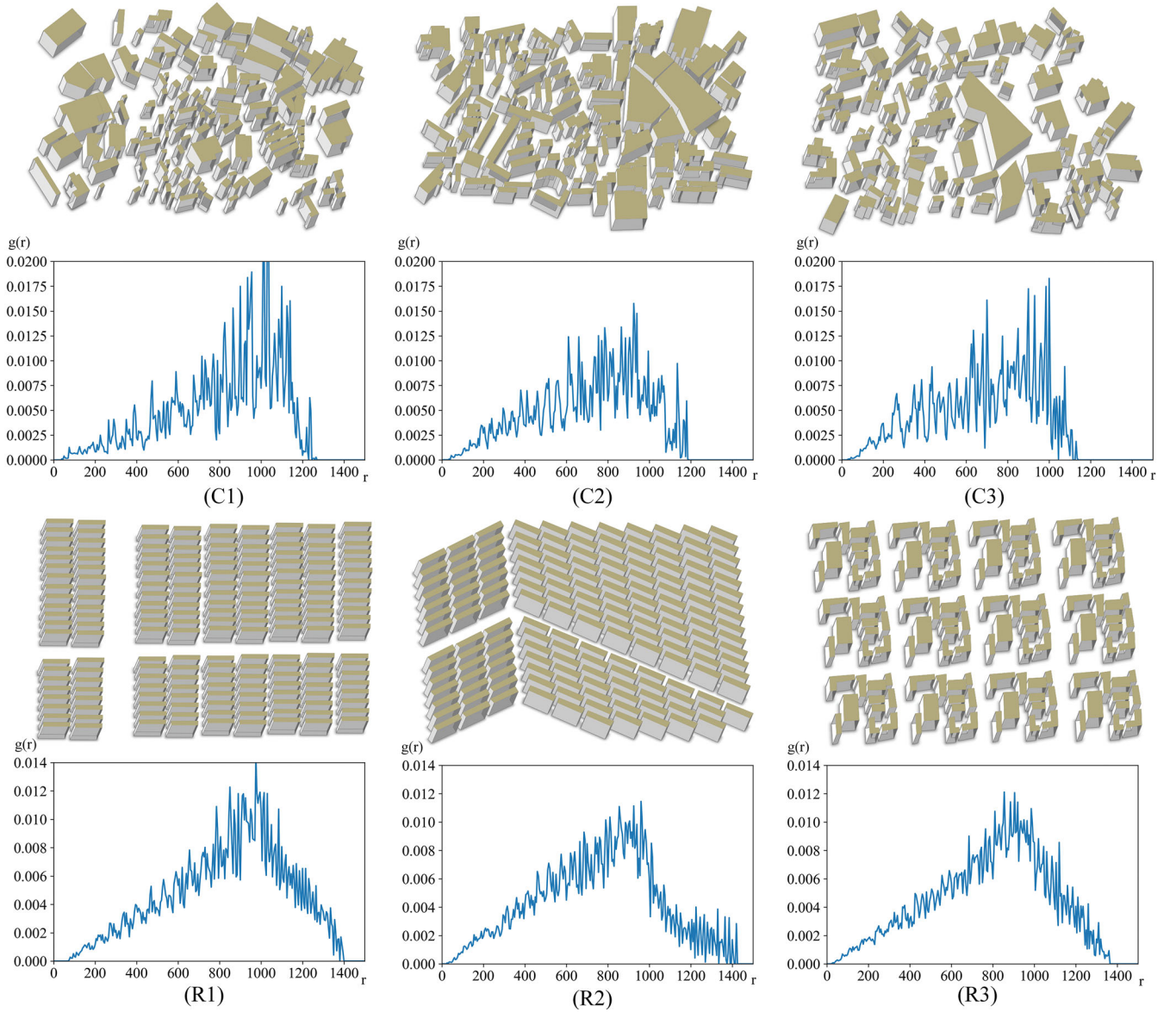


Figure 7. Texture curves of single-cluster building groups that are arranged with low regularities (C1, C2, and C3) and high regularities (R1, R2, and R3).

Texture Curves of Single-Cluster Building Groups with Varying Regularities and Heights. Similar to the simulated data set, the texture curves of the R-type building groups in Wuhan have more distinct peaks and smoother shapes like those of crystals, whereas the curves of C-type groups have larger fluctuations and no obvious peaks like the ones of fluids (Figure 10). Additionally, the curves of H-type building groups are smoother than those of L-type groups.

As shown in Table 2, the quantitative features extracted from the texture curves can greatly help differentiate various texture morphologies of local

urban landscapes. With respect to the data features, the burst statistics (B) and Shannon entropy values (Sh) of R-type building groups are smaller than those of C-type groups. Additionally, the coefficient of variation (CV) of an R-type building group is less than 1, whereas that of a C-type group is larger than 1. These features indicate that the $g(r)$ values of R-type building groups are regular and orderly. With respect to the curve features, the kurtosis (K) and skewness (Sk) of the C-type groups are much higher than those of R-type groups, indicating that the overall difference of the $g(r)$ results from the R-type groups is smaller than that from the C-type groups;

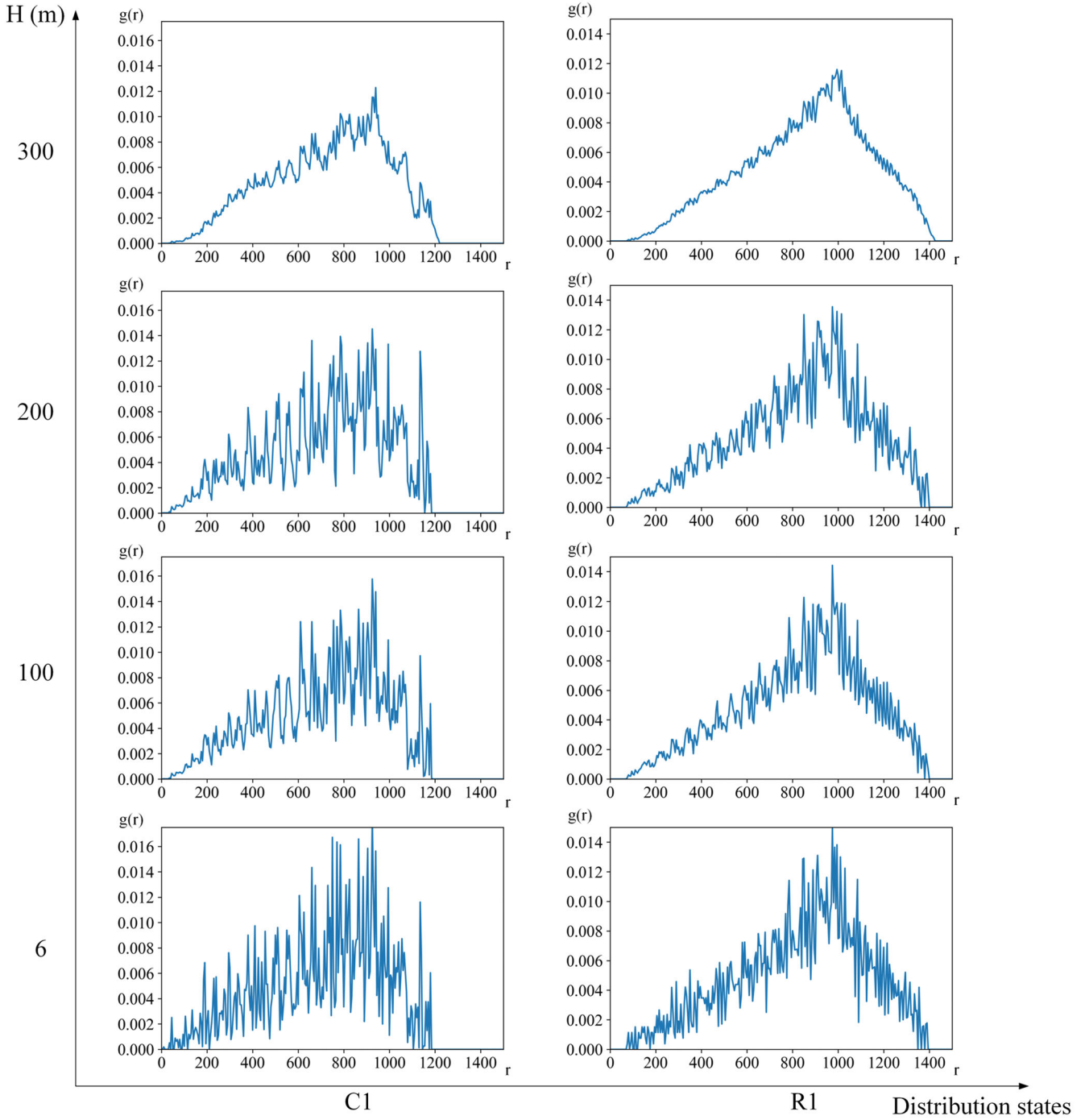


Figure 8. Texture curves of single-cluster building groups with different heights.

thus, the C-type groups' $g(r)$ results are more irregular.

In addition, the B, CV, K, and Sk of H-type groups are relatively larger than those of L-type groups. Compared with the H-type groups, the features of the L-type groups are more regular and orderly.

The first peak (FP) represents the radius of the building cluster that is closest to the spherical center, and the first peak area (FPA) reflects the degree of integration among the buildings inside the cluster. The FPs are shown in Table 2, and the value that is defined here indicates that a tight building cluster is formed within this radius. At the same building

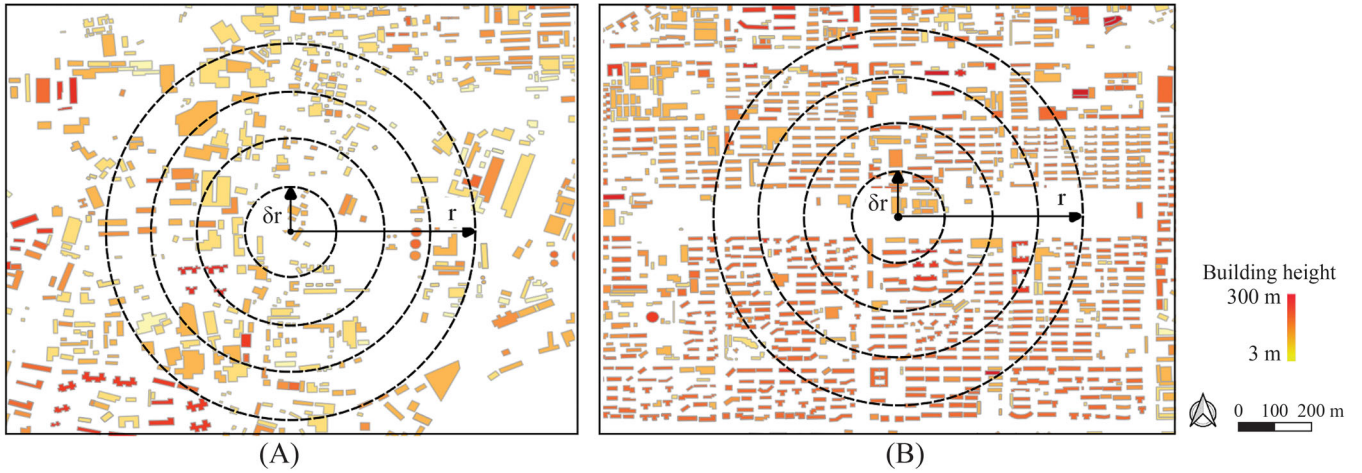


Figure 9. Examples of building groups that are arranged with (A) low regularity or (B) high regularity in Wuhan. The concentric circles represent the ground coverages of domes for the radial distribution function–based model. δr is the radius interval, and r is the maximum radius.

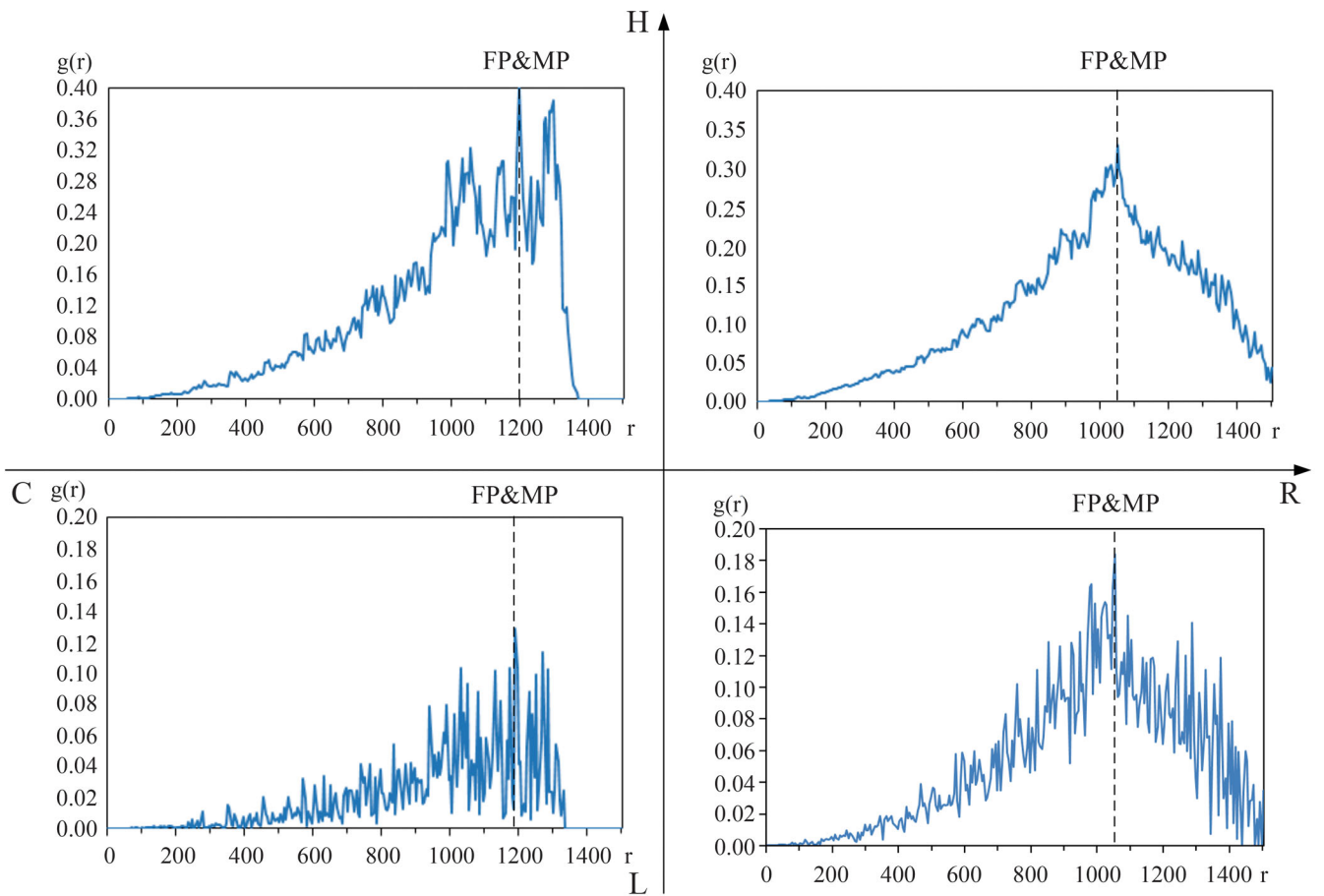


Figure 10. Texture curves of single-cluster building groups. Note: C=buildings are arranged with low regularity; R=buildings are arranged with high regularity; H=group includes mostly high-rise buildings; L=group includes mainly low-rise buildings; FP=position where the first peak of the curve appears; MP=position where the largest peak of the curve appears.

Table 2. Feature values of single-cluster building groups

	Data features			Curve features						
	CV	B	Sh	Sk	K	FP	MP	FPA	MPA	Tg
RL	0.92	0.05	3.35	0.83	2.89	1,045	1,045	80.56	80.56	—
RH	0.80	0.01	7.60	0.48	1.77	1,050	1,050	153.21	153.21	—
CL	1.82	0.25	8.18	1.80	5.00	1,185	1,185	67.94	67.94	—
CH	1.18	0.17	14.69	1.27	3.72	1,195	1,195	125.60	125.60	—

Note: CV=coefficient of variation; B=burst statistics; Sh=Shannon's entropy; Sk=skewness; K=kurtosis; FP=first peak; MP=maximum peak; FPA=first peak area; MPA=maximum peak area; Tg=transition point; RL=low-rise buildings that are arranged with high regularity; RH=high-rise buildings that are arranged with high regularity; CL=low-rise buildings that are arranged with low regularity; CH=high-rise buildings that are arranged with low regularity.

height, the FPA of an R-type group is larger than that of a C-type group, meaning the tightness among buildings in a R-type group is stronger than that of a C-type group. For single-cluster building groups, only one peak exists; hence, the FP and maximum peak (MP) are the same as the FPA and maximum peak area (MPA), and the transition points (Tgs) are null because no valley exists.

Texture Curves of Multicenter Building Groups with Varying Regularities and Heights. In a city, a local urban landscape might include one or more clusters of buildings. A multicenter building group at a certain location is composed of multiple clusters of buildings, and each cluster includes a set of closely distributed buildings that are relatively distant from other clusters. The urban texture model can also be used to describe the 3D characteristics of multicenter building groups, for which the texture curves might consist of multiple peaks and valleys (Figure 11). The curves of the R-type building groups have sharper peaks and are undulating. The $g(r)$ s of the C-type groups oscillate more and the curves fluctuate more. As the height of the building increases, the curves tend to be smoother.

Table 3 shows the features of multicenter building groups. The results show that multicenter building groups have almost the same tendency as single-cluster ones. For the curve features, due to the existence of multiple clusters, the degree of disorder in the group increases, so K and Sk increase. In general, the feature values of the R-type groups are smaller than those of the C-type groups. The MP represents the location of the most significant peak in the curve, and it is used to define the extent of a building cluster in the multicenter building group. From

the results of the FPA and MPA, the degree of integration in an R-type group is stronger than that in a C-type group. Additionally, the FPA and MPA of H-type groups are higher than those of L-type groups, indicating that the tightness of H-type groups is stronger than that of L-type groups.

A large Tg denotes that a “covalent bond” exists among the buildings and the dependence among the buildings is strong. In this study, the buildings in an R-type group are regularly arranged and there is a strong dependence among the buildings; therefore, the Tg is significant. Conversely, the buildings in a C-type group are irregularly arranged and the dependence among the buildings is weak; therefore, the Tg is small. The Tg can be used as a key feature to distinguish between R-type and C-type groups in a multicenter urban landscape.

Urban Texture Morphologies in the Study Area

The proposed model is able to quantitatively characterize the texture morphologies of local urban landscapes at various locations in a city and effectively distinguish various morphological patterns in a complex urban area. We randomly selected 10,000 locations in the downtown area of Wuhan and used the proposed model to calculate the texture features of all building groups at the selected locations within a 500 m radius. These building groups were classified into four typical morphological types (RH/RL/CH/CL), as shown in Figure 12.

A large proportion of the randomly selected locations exhibit either RH or CL texture morphologies. RH morphologies are primarily located in the mature commercial areas along the Yangtze River and newly developed residential areas along the urban edges, where high-rise commercial and residential buildings have been developed with rigorous planning. CL morphologies are concentrated in the northeast part of the study area, where many industrial plants and small villages are located. CH morphologies are mostly found at the locations between RH and CL, where urban renewal is in progress and newly built high-rise buildings are scattered in old town landscapes. Notably, the heights of buildings around the Yellow Crane Tower (the location is marked in Figure 12) are highly restricted, so a large number of RL and CL morphologies are located in this area. Such a spatial distribution pattern of urban texture morphologies reflects the complex landscapes and

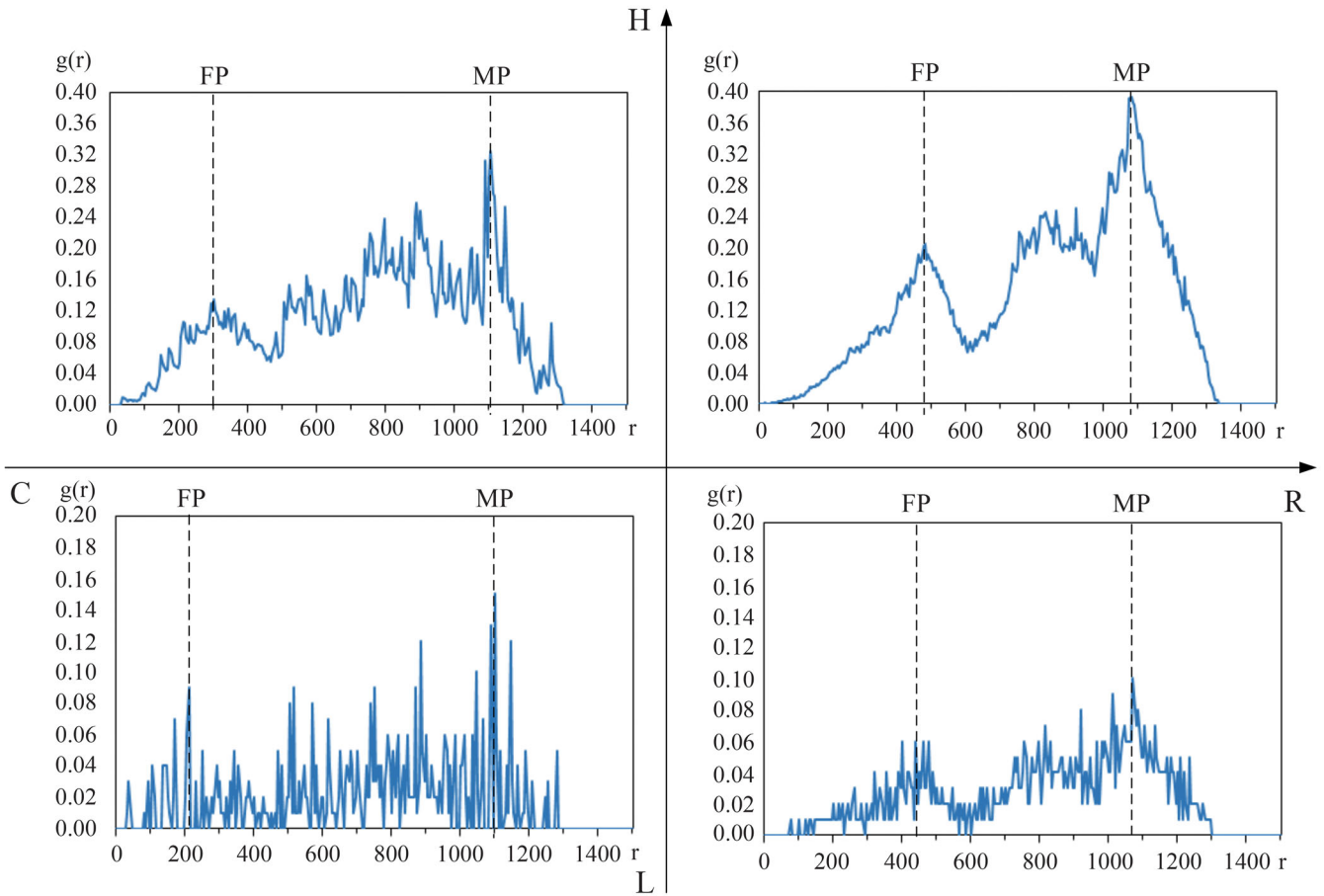


Figure 11. Texture curves of multicluster building groups. *Note:* C=buildings are arranged with low regularity; R=buildings are arranged with high regularity; H=group includes mostly high-rise buildings; L=group includes mainly low-rise buildings; FP=position where the first peak of the curve appears; MP=position where the largest peak of the curve appears.

Table 3. Feature values of multicluster building groups.

	Data features			Curve features						
	CV	B	Sh	Sk	K	FP	MP	FPA	MPA	Tg
RL	0.88	0.11	10.38	1.04	4.02	440	1070	35.69	89.12	2.14
RH	0.62	0.07	27.17	0.98	3.35	485	1085	90.78	241.35	2.51
CL	1.60	0.53	13.03	2.60	11.02	210	1100	17.84	56.44	1.38
CH	1.11	0.15	16.56	2.28	6.41	300	1105	50.79	195.82	1.76

Note: CV=coefficient of variation; B=burst statistics; Sh=Shannon’s entropy; Sk=skewness; K=kurtosis; FP=first peak; MP=maximum peak; FPA=first peak area; MPA=maximum peak area; Tg=transition point; RL=low-rise buildings that are arranged with high regularity; RH=high-rise buildings that are arranged with high regularity; CL=low-rise buildings that are arranged with low regularity; CH=high-rise buildings that are arranged with low regularity.

the development progress of the downtown area of Wuhan, providing key information for the evaluation of local environment and decision making in urban planning.

Relationship between 3D Texture Features and LST

The 3D texture morphology of an urban landscape has a significant impact on the local environment. We used the quantitative features extracted by the proposed 3D texture model to estimate the LST at the 10,000 randomly selected locations, through an RFR model. Also, to provide a baseline for the performance assessment, we used a 2D texture model to estimate the local LST as well. Instead of a set of concentric domes above the ground, the 2D model uses a set of concentric 2D circles on the ground to characterize the spatial arrangement of buildings in a 2D space (as in Sobstyl et al. 2018), which means the height variations of buildings are ignored.

A series of experiments was conducted using various radius intervals for the concentric domes or circles (as mentioned earlier, even though the radius

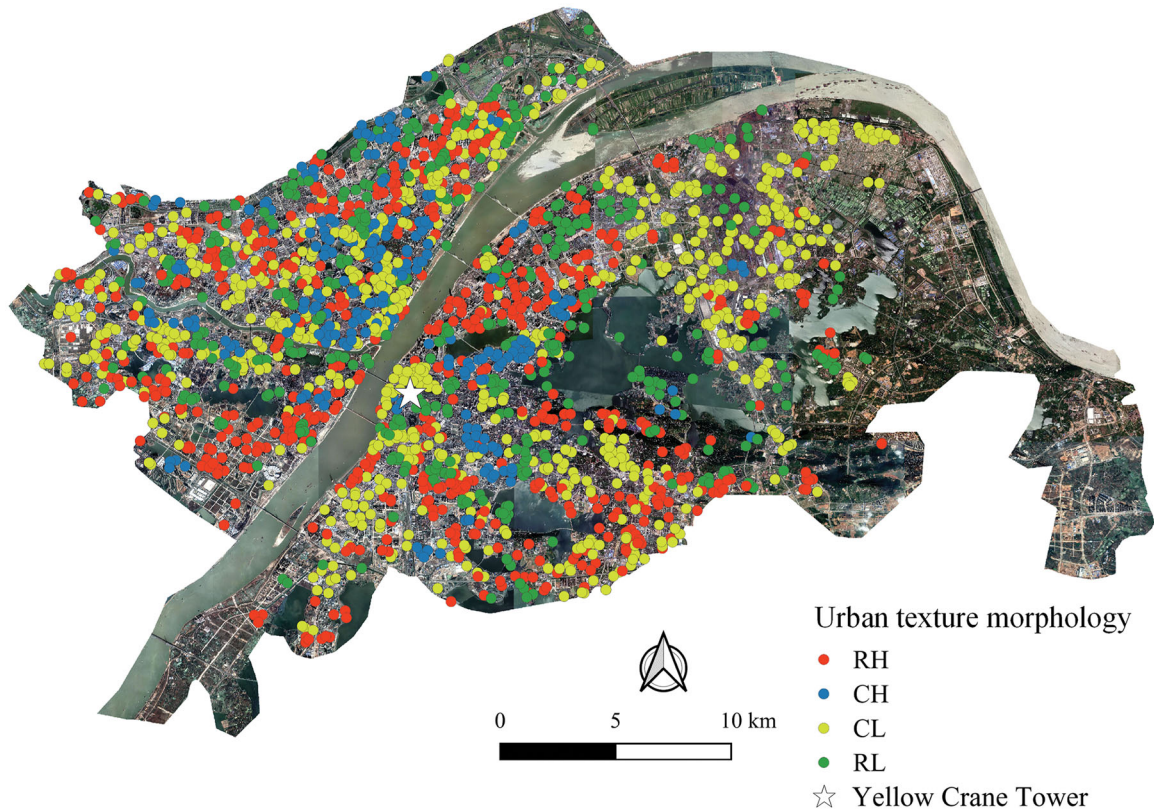


Figure 12. Texture morphologies of the 10,000 random locations in Wuhan. *Note:* RH=high-rise buildings that are arranged with high regularity; CH=high-rise buildings that are arranged with low regularity; CL=low-rise buildings that are arranged with low regularity; RL=low-rise buildings that are arranged with high regularity.

intervals in these experiments are different, the maximum range of the LCZ remains the same at 500 m, so the number of concentric circles will change accordingly). As shown in Figure 11A, the fitting accuracy (R^2) of the 3D model is better than that of the 2D model at every radius interval. When the radius interval is 50 m, the accuracy of the 3D model reaches the maximum at 0.639, a 12.7 percent improvement over the accuracy of the 2D model (0.567). Such results indicate that the 3D texture morphological features by the proposed model carry critical information for the local LST that the 2D model is unable to fully capture. The model considering the heights of the buildings can describe the overall characteristics of buildings more accurately in the urban canopy (Chun 2011; Berger et al. 2017). Therefore, the proposed model effectively revealed the correlation between the 3D morphology of urban buildings and the thermal environment within a city.

Figure 13 also shows that for both the 2D and 3D models, with the increase of radius intervals, the fitting accuracy increases to the maximum value and then decreases. When the radius interval is 50 m,

the 3D texture features quantified by this model can explain the difference in LST with a correlation of 0.639, which means that these 3D spatial morphological characteristics of buildings are important factors influencing the differences in the LSTs within the city. It indicates that at a granularity of 50 m, the features quantified in this study have a high correlation with the surface temperature.

Discussion

The Importance of Texture Features to Affect LST

One of the key advantages of the RFR method is the capability of providing the importance of each feature to the target variable (i.e., the LST in this case). As shown in Figure 14, CV, Tg, FPA, and MPA of the texture curve contribute the most to the LST fitting, followed by B, K, MP, and Sk. The FP and Sh values contribute the least to the fitting result.

CV and Tg are the two most important features that characterize the degree of regularity of the

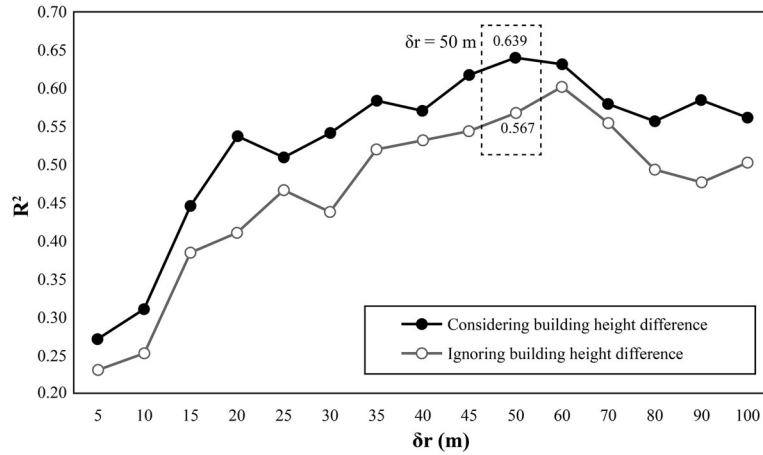


Figure 13. Land surface temperature fitting accuracies (R_2) of the proposed 3D model and the 2D model with varying radius intervals.

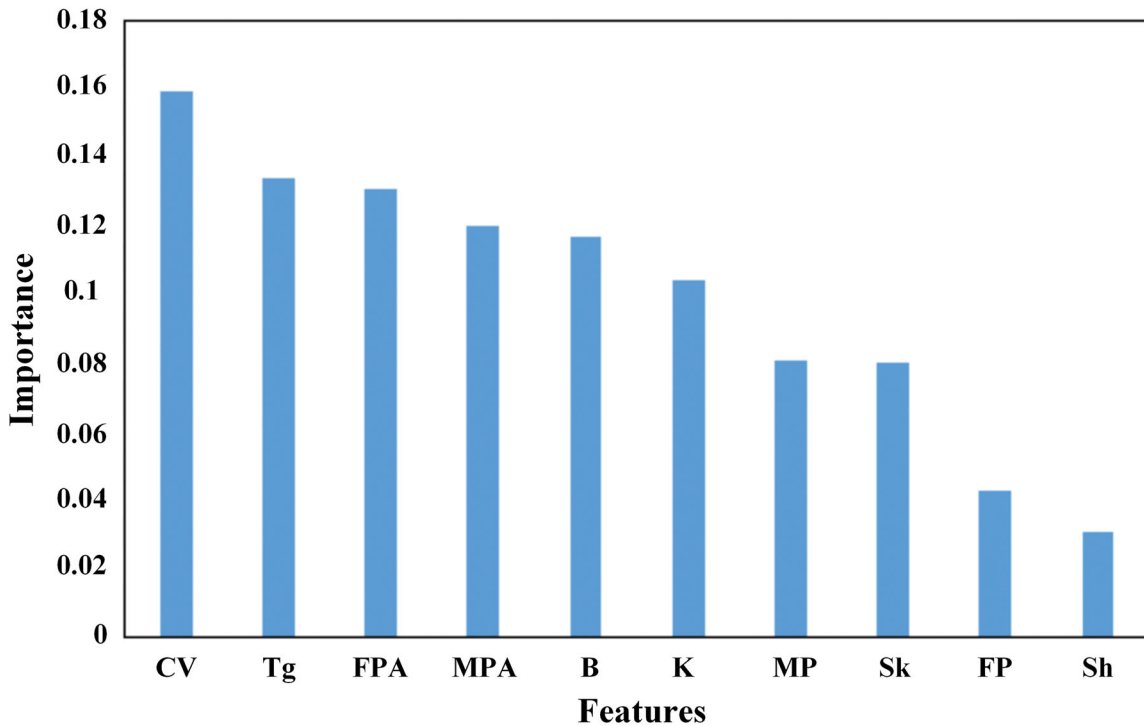


Figure 14. Importance ranking of the features. Note: CV=coefficient of variation; Tg=transition point; FPA=first peak area; MPA=maximum peak area; B=burst statistics; K=kurtosis; MP=maximum peak; Sk=skewness; FP=first peak; Sh=Shannon’s entropy.

building group and quantitatively reflect the spatial distribution of the building groups. A distribution with a CV greater than 1 is a distribution with high differences. The larger that Tg is, the stronger the dependence between particles. The MPA and FPA can also reflect the density of the buildings in the local landscape, in addition to reflecting the interdependence of the buildings. A larger MPA means that the center building has more “coordination” under the dome, which indicates that the building density is greater.

These findings from the perspective of the texture morphology are consistent with the conclusions from other studies that the density of the buildings has a strong correlation with the LST (Guo et al. 2016).

Comparison with State-of-the-Art 3D Feature Extraction Models

To further assess the performance of the proposed 3D texture model in revealing the correlation

Table 4. Accuracy comparison for the state-of-the-art building–land surface temperature models

Models	Fitting accuracy (R^2)
Building density and heights (Model 1)	0.373
Sky view factor (Model 2)	0.507
Spatial fluctuation factors (Model 3)	0.428
3D landscape factors (Model 4)	0.541
The proposed RDF-based model	0.639

Note: RDF = radial distribution function.

between urban landscape and LST, this study also applied several state-of-the-art models in the study area to extract various 3D features of buildings at the same scale (50 m), including building density and heights (Guo et al. 2016), sky view factor (L. Chen et al. 2012), spatial fluctuation factors (P. Zhang 2016), and 3D landscape factors (J. Yang et al. 2017). These features were then used to estimate the LST at the 10,000 locations in the study area through the RFR method. The fitting accuracies (R^2) of these models are shown in Table 4.

Model 1 does not achieve good accuracy because simply calculating the effects of the building density and heights is not sufficient to accurately estimate the urban temperature (Berger et al. 2017). Model 2 considers the effects of the street view around a building and achieves a better result than Model 1. Although the street condition is an important factor that affects the temperature between buildings, the morphological characteristics of buildings are ignored in Model 2. The proposed RDF-based model can quantitatively describe the morphological characteristics of buildings around any location and improve the fitting accuracy by 26.0 percent to 71.3 percent.

The spatial fluctuation factors and 3D landscape factors of the buildings can reveal their 3D morphological characteristics from different angles (e.g., undulation, building otherness, floor area ratio; Preez 2015). Both Model 3 and Model 4 are more comprehensive than Model 1 and Model 2 and achieve better fitting accuracies. They cannot reflect the 3D distribution state (e.g., tightness of distribution, degree of regularity) of the buildings, however, which is an important factor affecting the urban temperature (Sobstyl et al. 2018). By making an analogy between the buildings and the particles in the microscopic system, the proposed RDF-based model summarizes both the 3D landscape features and the distribution arrangement of the buildings. Compared with the state-of-the-art models that

consider buildings' 3D morphological characteristics, the proposed RDF-based model improved the fitting accuracy by 18.11 percent to 49.29 percent.

Conclusions

To quantitatively characterize the 3D texture morphology of buildings, this study proposes a 3D urban texture model based on the RDF. By using a set of concentric domes above the ground, the model generates a texture curve for a specific location in the city, from which a variety of numerical features are extracted to depict the local 3D urban landscape quantitatively. The experiments on both a simulated data set and a Wuhan data set showed that the proposed model can effectively distinguish various 3D texture morphologies of buildings at any location in a city. The 3D texture features extracted by the proposed model were used to estimate the LST at 10,000 randomly selected locations in Wuhan and improved the fitting accuracy by 12.7 percent compared with the 2D RDF-based model and by 18.11 percent to 71.3 percent compared with several state-of-the-art 3D feature extraction models.

The proposed RDF-based 3D urban texture model provides a new perspective and approach to effectively depict 3D urban landscapes at fine scales with a set of simple and straightforward indexes, which enables numerical computations and analysis of complex urban morphologies. Such a 3D texture model can be used in a wide range of urban studies and applications. For example, various spatial patterns of building groups can be differentiated and compared within a city or across cities, providing essential information for urban planning and building design. In addition, the 3D texture morphology of buildings provides a basis for the analysis of an urban environment. The correlations between urban texture and various environmental variables (e.g., ventilation, humidity, air quality, noise, and light) can be analyzed to discover the mechanism of the urban landscape's effects on the environment and to derive measures to mitigate citizens' exposure to environmental pollution and improve living comfort. More important, by replacing buildings with other elements of the city (e.g., air pollution, meteorological variables), the proposed RDF-based model can also be applied to quantify the 3D texture morphology of these elements, effectively characterizing the 3D distribution of the elements in a complex urban system.

In follow-up research, we will combine multisource spatiotemporal data and apply the model to other aspects of urban research (e.g., urban LCZ, urban perception) for further analysis of the 3D texture of the city. To accurately quantify the texture morphology of buildings, we will use the true shape of the building to estimate the precise building density. By comparing the LST data of different seasons and periods, we will further explore the correlation between urban texture and urban climate and environment. Also, we will enhance the LST fitting accuracy by considering additional factors such as traffic networks and flows, water bodies, and vegetation coverage.

Acknowledgments

Dr. Yao Yao and Ms. Teng Ma served as the corresponding authors for this article. We sincerely thank the editors and anonymous reviewers for their constructive comments and suggestions.

Funding

This work was supported by the National Key Research and Development Program of China (Grant No. 2019YFB2102903), the National Natural Science Foundation of China (Grant No. 41801306, 42171466) and the Scientific Research Program of the Department of Natural Resources of Hubei Province (Grant No. ZRZY2021KJ02).

ORCID

Qingfeng Guan  <http://orcid.org/0000-0002-7392-3709>

Yao Yao  <http://orcid.org/0000-0002-2830-0377>

Jianjun Lyu  <http://orcid.org/0000-0002-8144-1929>

References

- Ai, T., and X. Zhang. 2007. The aggregation of urban building clusters based on the skeleton partitioning of gap space. *Lecture Notes in Geoinformation & Cartography* 2007:153–70.
- Berger, C., J. Rosentreter, M. Voltersen, C. Baumgart, C. Schullius, and S. Hese. 2017. Spatio-temporal analysis of the relationship between 2D/3D urban site characteristics and land surface temperature. *Remote Sensing of Environment* 193:225–43. doi: 10.1016/j.rse.2017.02.020.
- Bragg, W. L., and H. Lipson. 1938. Structure of metals. *Nature* 141 (3565):367–68. doi: 10.1038/141367a0.
- Breiman, L. 2001. Random forests. *Machine Learning* 45 (1):5–32. doi: 10.1023/A:1010933404324.
- Brian, S. 2008. Urban sprawl and air quality in large U.S. cities. *Journal of Environmental Management* 86 (4):688–98.
- Brown, C. E. 2011. Coefficient of variation. *Encyclopedia of Statistical Sciences* 94 (1):94.
- Burgot, J. 2017. Radial distribution function. In *The notion of activity in chemistry*, 329–35. Cham, Switzerland: Springer.
- Chen, L., E. Ng, X. An, C. Ren, M. Lee, U. Wang, and Z. He. 2012. Sky view factor analysis of street canyons and its implications for daytime intra-urban air temperature differentials in high-rise, high-density urban areas of Hong Kong: A GIS-based simulation approach. *International Journal of Climatology* 32 (1):121–36. doi: 10.1002/joc.2243.
- Chen, Z., and Y. C. Soh. 2014. Modeling building occupancy using a novel inhomogeneous Markov chain approach. Paper presented at the IEEE International Conference on Automation Science & Engineering. New Taipei, Taiwan. August, 2014. 1079–1084.
- Cherkas, N. L., and S. L. Cherkas. 2016. Model of the radial distribution function of pores in a layer of porous aluminum oxide. *Crystallography Reports* 61 (2):285–90. doi: 10.1134/S106377451506005X.
- Chun, B. S. 2011. Three-dimensional city determinants of the urban heat island: A statistical approach. Dissertations & Theses, Gradworks.
- Cutler, A., D. R. Cutler, and J. R. Stevens. 2011. Random forests. *Machine Learning* 45 (1):157–76.
- Dobinson, S. C. 1993. *Studies in Romano-British urban structure: A consideration of aspects of planning, building stock and internal structure of the major towns of Roman Britain*. Cambridge, UK: University of Cambridge.
- Eduardo, W. 2006. The radial distribution function for a fluid of hard spheres at high densities. *Molecular Physics* 25 (1):45–48. doi: 10.1080/00268977300100061.
- Ellefsen, R. 1991. Mapping and measuring buildings in the canopy boundary layer in ten U.S. sites. *Energy and Buildings* 16 (3–4):1025–49. doi: 10.1016/0378-7788(91)90097-M.
- Gaetano, R., G. Scarpa, and G. Poggi. 2009. Hierarchical texture-based segmentation of multiresolution remote-sensing images. *IEEE Transactions on Geoscience and Remote Sensing* 47 (7):2129–41. doi: 10.1109/TGRS.2008.2010708.
- Goh, K. I., and A. L. Barabási. 2012. Burstiness and memory in complex systems. *Physics* 81 (4):23–25.
- Grömping, U. 2009. Variable importance assessment in regression: Linear regression versus random forest. *American Statistician* 63 (4):308–19. doi: 10.1198/tast.2009.08199.
- Guo, G., X. Zhou, Z. Wu, R. Xiao, and Y. Chen. 2016. Characterizing the impact of urban morphology heterogeneity on land surface temperature in Guangzhou, China. *Environmental Modelling & Software* 84:427–39. doi: 10.1016/j.envsoft.2016.06.021.
- He, Y., B. Ai, Y. Yao, and F. Zhong. 2015. Deriving urban dynamic evolution rules from self-adaptive cellular automata with multi-temporal remote sensing

- images. *International Journal of Applied Earth Observation and Geoinformation* 38:164–74. doi: [10.1016/j.jag.2014.12.014](https://doi.org/10.1016/j.jag.2014.12.014).
- He, Z., M. Deng, J. Cai, Z. Xie, Q. Guan, and C. Yang. 2020. Mining spatiotemporal association patterns from complex geographic phenomena. *International Journal of Geographical Information Science* 34 (6):1162–87.
- Heinzel, J., and T. Kemper. 2015. Automated metric characterization of urban structure using building decomposition from very high resolution imagery. *International Journal of Applied Earth Observation and Geoinformation* 35:151–60. doi: [10.1016/j.jag.2014.08.017](https://doi.org/10.1016/j.jag.2014.08.017).
- Hutengs, C., and M. Vohland. 2016. Downscaling land surface temperatures at regional scales with random forest regression. *Remote Sensing of Environment* 178:127–41. doi: [10.1016/j.rse.2016.03.006](https://doi.org/10.1016/j.rse.2016.03.006).
- Inostroza, L., R. Baur, and E. Csaplovics. 2013. Urban sprawl and fragmentation in Latin America: A dynamic quantification and characterization of spatial patterns. *Journal of Environmental Management* 115 (3):87–97. doi: [10.1016/j.jenvman.2012.11.007](https://doi.org/10.1016/j.jenvman.2012.11.007).
- Ivanova, S. M. 2015. 3D analysis of the incident diffuse irradiance on the building's surfaces in an urban environment. *International Journal of Low-Carbon Technologies* 10 (3):262–67. doi: [10.1093/ijlct/ctu001](https://doi.org/10.1093/ijlct/ctu001)
- Jian, H., L. Yuguo, R. Sandberg, R. Buccolieri, and S. Di Sabatino. 2012. The influence of building height variability on pollutant dispersion and pedestrian ventilation in idealized high-rise urban areas. *Building & Environment* 56 (10):346–60.
- Kharchenko, S. 2016. City location on the river network pattern and the effect of relief on the distribution of urban buildings. *Research Journal of Pharmaceutical Biological & Chemical Sciences* 7 (5):1543–49.
- Kim, J., D. K. Lee, W. Jeong, S. Sung, and J. Park. 2015. The urban heat island impact in consideration of spatial pattern of urban landscape and structure. Paper presented at the American Geophysical Union Fall meeting, San Francisco, CA, December 2015. 2015: B33E-0763.
- Kramer, O. 2016. *Scikit-Learn*. New York: Springer International.
- Kumar, M., and E. Tretkoff. 2010. Research spotlight: Climate change and urbanization increase urban heat island effect. *Eos: Transactions of the American Geophysical Union* 91 (27):244. doi: [10.1029/EO091i027p00244-02](https://doi.org/10.1029/EO091i027p00244-02).
- Leconte, F., J. Bouyer, R. Claverie, M. Pétrissans, F. Leconte, J. Bouyer, and M. Pétrissans. 2015. Using local climate zone scheme for UHI assessment: Evaluation of the method using mobile measurements. *Building and Environment* 83:39–49. doi: [10.1016/j.buildenv.2014.05.005](https://doi.org/10.1016/j.buildenv.2014.05.005).
- Li, Z., W. Shi, H. Ming, and Z. Hua. 2017. Unsupervised change detection using spectral features and a texture difference measure for VHR remote-sensing images. *International Journal of Remote Sensing* 38 (23):7302–15. doi: [10.1080/01431161.2017.1375616](https://doi.org/10.1080/01431161.2017.1375616).
- Luo, X., and W. Li. 2014. Scale effect analysis of the relationships between urban heat island and impact factors: Case study in Chongqing. *Journal of Applied Remote Sensing* 8 (1):084995–292. doi: [10.1117/1.JRS.8.084995](https://doi.org/10.1117/1.JRS.8.084995).
- Manesh, S. V., and M. Tadi. 2011. Sustainable urban morphology emergence via complex adaptive system analysis: Sustainable design in existing context. *Procedia Engineering* 21:89–97. doi: [10.1016/j.proeng.2011.11.1991](https://doi.org/10.1016/j.proeng.2011.11.1991).
- Mardia, K. V. 1970. Measures of multivariate skewness and kurtosis with applications. *Biometrika* 57 (3):519–30. doi: [10.1093/biomet/57.3.519](https://doi.org/10.1093/biomet/57.3.519).
- Palme, M., L. Inostroza, and A. Salvati. 2018. Technomass and cooling demand in South America: A superlinear relationship? *Building Research & Information* 46 (8):864–80. doi: [10.1080/09613218.2018.1483868](https://doi.org/10.1080/09613218.2018.1483868).
- Pan, X. Z., Q. G. Zhao, J. Chen, Y. Liang, and B. Sun. 2008. Analyzing the variation of building density using high spatial resolution satellite images: The example of Shanghai city. *Sensors* 8 (4):2541–50. doi: [10.3390/s8042541](https://doi.org/10.3390/s8042541).
- Perini, K., and A. Magliocco. 2014. Effects of vegetation, urban density, building height, and atmospheric conditions on local temperatures and thermal comfort. *Urban Forestry & Urban Greening* 13 (3):495–506. doi: [10.1016/j.ufug.2014.03.003](https://doi.org/10.1016/j.ufug.2014.03.003).
- Preez, C. D. 2015. A new arc-chord ratio (ACR) rugosity index for quantifying three-dimensional landscape structural complexity. *Landscape Ecology* 30 (1):181–92.
- Qin, J., C. Fang, Y. Wang, G. Li, and S. Wang. 2015. Evaluation of three-dimensional urban expansion: A case study of Yangzhou city, Jiangsu province, China. *Chinese Geographical Science* 25 (2):224–36. doi: [10.1007/s11769-014-0728-8](https://doi.org/10.1007/s11769-014-0728-8).
- Quattrochi, D. 2013. *Climate interactions with the built environment in the Southeast USA*. Washington, DC: Island Press/Center for Resource Economics.
- Roman, K. K., T. O'Brien, J. B. Alvey, and O. J. Woo. 2016. Simulating the effects of cool roof and PCM (phase change materials) based roof to mitigate UHI (urban heat island) in prominent U.S. cities. *Energy* 96:103–17. doi: [10.1016/j.energy.2015.11.082](https://doi.org/10.1016/j.energy.2015.11.082).
- Rykwert, J. 1988. Off limits: City pattern and city texture. *RSA Journal* 136 (5388):897–911.
- Shannon, C. E., W. Weaver, and N. Wiener. 1949. *The mathematical theory of communication*. University of Illinois Press.
- Sobstyl, J. M., T. Emig, M. J. A. Qomi, F.-J. Ulm, and R. J.-M. Pellenq. 2018. Role of city texture in urban heat islands at nighttime. *Physical Review Letters* 120 (10):108701. doi: [10.1103/PhysRevLett.120.108701](https://doi.org/10.1103/PhysRevLett.120.108701).
- Sossa, A. S., C. Curtis, M. Karimi, B. Vanthull, R. Khanbilvardi, and R. Nazari. 2013. *Establishing a correlation between the urban heat island (UHI) effect in New York City and the land cover*. Washington, DC: American Geophysical Union.
- Stewart, I. D., and T. R. Oke. 2012. Local climate zones for urban temperature studies. *Bulletin of the American Meteorological Society* 93 (12):1879–900. doi: [10.1175/BAMS-D-11-00019.1](https://doi.org/10.1175/BAMS-D-11-00019.1).
- Strømmand-Andersen, J., and P. A. Sattrup. 2011. The urban canyon and building energy use: Urban density versus daylight and passive solar gains. *Energy and Buildings* 43 (8):2011–20. doi: [10.1016/j.enbuild.2011.04.007](https://doi.org/10.1016/j.enbuild.2011.04.007).

- Su, Y. F., G. M. Foody, and K. S. Cheng. 2012. Spatial non-stationarity in the relationships between land cover and surface temperature in an urban heat island and its impacts on thermally sensitive populations. *Landscape and Urban Planning* 107 (2):172–80. doi: [10.1016/j.landurbplan.2012.05.016](https://doi.org/10.1016/j.landurbplan.2012.05.016).
- Sukhomlinov, S. V., and M. H. Müser. 2017. Determination of accurate, mean bond lengths from radial distribution functions. *Journal of Chemical Physics* 146 (2):24506.
- Wang, M., Z. Zhang, T. Hu, and X. Liu. 2019. A practical single-channel algorithm for land surface temperature retrieval: Application to Landsat series data. *Journal of Geophysical Research: Atmospheres* 124 (1):299–316.
- Wentz, E. A., A. M. York, A. Marina, C. Lindsey, F. Heather, I. Luis, J. Claire, S. T. A. Pickett, K. C. Seto, and T. C. Hannes. 2018. Six fundamental aspects for conceptualizing multidimensional urban form: A spatial mapping perspective. *Landscape and Urban Planning* 179:55–62. doi: [10.1016/j.landurbplan.2018.07.007](https://doi.org/10.1016/j.landurbplan.2018.07.007).
- Xian, G. 2008. Satellite remotely-sensed land surface parameters and their climatic effects for three metropolitan regions. *Advances in Space Research* 41 (11):1861–69. doi: [10.1016/j.asr.2007.11.004](https://doi.org/10.1016/j.asr.2007.11.004).
- Yang, J., A. Guo, J. Xi, Q. Ge, and X. Li. 2017. Spatial-temporal differentiation of three-dimensional urban landscape pattern: A case study of Zhongshan district in Dalian. *Acta Geographica SINICA* 72 (4):646–56.
- Yang, X., and Y. Li. 2013. Development of a three-dimensional urban energy model for predicting and understanding surface temperature distribution. *Boundary-Layer Meteorology* 149 (2):303–21. doi: [10.1007/s10546-013-9842-x](https://doi.org/10.1007/s10546-013-9842-x).
- Yang, X., and Y. Li. 2015. The impact of building density and building height heterogeneity on average urban albedo and street surface temperature. *Building and Environment* 90:146–56. doi: [10.1016/j.buildenv.2015.03.037](https://doi.org/10.1016/j.buildenv.2015.03.037).
- Yin, C., M. Yuan, Y. Lu, Y. Huang, and Y. Liu. 2018. Effects of urban form on the urban heat island effect based on spatial regression model. *The Science of the Total Environment* 634:696–704. doi: [10.1016/j.scitotenv.2018.03.350](https://doi.org/10.1016/j.scitotenv.2018.03.350).
- Yu, B., H. Liu, J. Wu, Y. Hu, and L. Zhang. 2010. Automated derivation of urban building density information using airborne LiDAR data and object-based method. *Landscape and Urban Planning* 98 (3–4):210–19. doi: [10.1016/j.landurbplan.2010.08.004](https://doi.org/10.1016/j.landurbplan.2010.08.004).
- Yu, S., B. Yu, W. Song, B. Wu, J. Zhou, Y. Huang, J. Wu, F. Zhao, and W. Mao. 2016. View-based greenery: A three-dimensional assessment of city buildings' green visibility using Floor Green View Index. *Landscape and Urban Planning* 152:13–26. doi: [10.1016/j.landurbplan.2016.04.004](https://doi.org/10.1016/j.landurbplan.2016.04.004).
- Zhang, P. 2016. Spatial fluctuation of urban architecture. *Journal of Arid Land Resources and Environment* 30 (2):51–56.
- Zhang, Y., Y. Liu, Y. Zhang, Y. Liu, G. Zhang, and Y. Chen. 2018. On the spatial relationship between ecosystem services and urbanization: A case study in Wuhan, China. *The Science of the Total Environment* 637–638:780–90. doi: [10.1016/j.scitotenv.2018.04.396](https://doi.org/10.1016/j.scitotenv.2018.04.396).
- Zhu, J., and Y. Sun. 2017. Building an urban spatial structure from urban land use data: An example using automated recognition of the city centre. *ISPRS International Journal of Geo-Information* 6 (4):122. doi: [10.3390/ijgi6040122](https://doi.org/10.3390/ijgi6040122).

QINGFENG GUAN is a Professor at China University of Geosciences, Wuhan 430078, Hubei Province, China. E-mail: guanqf@cug.edu.cn. His research interests are high-performance spatial intelligence computation and urban computing.

YAO YAO is an Associate Professor at China University of Geosciences, Wuhan 430078, Hubei Province, China, and a Senior Algorithm Engineer at Alibaba Group. E-mail: yaoy@cug.edu.cn. His research interests are geospatial big data mining, analysis, and computational urban science.

TENG MA is a Graduate from the School of Geography and Information Engineering, China University of Geosciences, Wuhan 430078, Hubei Province, China. E-mail: tengzi@cug.edu.cn. She currently works at Amap, one of the largest online map providers in China, focusing on designing and building a platform for high-definition map data.

YE HONG is a PhD Candidate in the Institute of Cartography and Geoinformation at the Swiss Federal Institute of Technology (ETH) Zurich 8092, Switzerland. E-mail: hongy@ethz.ch. His research interests include spatiotemporal data analytics and mining, urban computing, and human mobility.

YONGPAN BIE obtained his Master's Degree from China University of Geosciences, Wuhan 430078, Hubei Province, China. E-mail: yongpanbie@163.com. His research interests are augmented reality visualization of geographic data and urban computing.

JIANJUN LYU is a Professor at China University of Geosciences, Wuhan 430078, Hubei Province, China. E-mail: jjlv@cug.edu.cn. His research interests are spatial structure evaluation and optimization of urban agglomerations and spatiotemporal big data analytics.